Contribution from the Departments of Chemistry, Rutgers, The State University of New Jersey, New Brunswick, New Jersey 08903, and Rutgers, The State University of New Jersey, Newark, New Jersey 07102

Molecular Structures, Electronic Spectra, and ESR Spectra of Bis(4,4′,5,5′-tetramethyl-2,2′-biimidazole)copper(II) Dinitrate and Bis(4,4′,5,5′-tetramethyl-2,2′-biimidazole)zinc(II)$_{0.90}$copper(II)$_{0.10}$ Dinitrate

ERNEST E. BERNARDUCCI,[1a] PARIMAL K. BHARADWAJ,[1a] ROGER A. LALANCETTE,*[1b] KARSTEN KROGH-JESPERSEN,*[1a] JOSEPH A. POTENZA,*[1a] and HARVEY J. SCHUGAR*[1a]

Received February 8, 1983

The crystal structures of bis(4,4′,5,5′-tetramethyl-2,2′-biimidazole)copper(II) dinitrate (**1**) and bis(4,4′,5,5′-tetramethyl-2,2′-biimidazole)zinc(II)$_{0.90}$copper(II)$_{0.10}$ dinitrate (**2**) have been determined from single-crystal X-ray data collected by counter methods. Complex **1** ($CuC_{20}H_{28}N_{10}O_6$) crystallized in space group $P\bar{1}$ with $Z = 2$ and $a = 7.854$ (1) Å, $b = 14.303$ (2) Å, $c = 11.852$ (2) Å, $\alpha = 78.46$ (2)°, $\beta = 94.96$ (2)°, and $\gamma = 91.92$ (1)°. Complex **2** ($Zn_{0.9}Cu_{0.1}C_{20}H_{28}N_{10}O_6$) also crystallized in $P\bar{1}$ with $Z = 2$ and $a = 7.812$ (1) Å, $b = 13.324$ (3) Å, $c = 13.692$ (3) Å, $\alpha = 72.72$ (2)°, $\beta = 107.00$ (1)°, and $\gamma = 96.77$ (1)°. Structure **1** consists of discrete $[Cu(Me_4BIM)_2ONO_2]^+$ cations separated by lattice NO_3^- groups. The anisobidentate NO_3^- ligand exhibits a normal Cu–O bond (2.180 (7) Å) as well as a longer Cu–O semibond (2.569 (8) Å). If the semibond is ignored, the distorted coordination geometry lies closer to the idealized square pyramid than to the idealized trigonal bipyramid. The coordination geometry is completed by three additional equatorial bonds to nitrogen donors (1.987 (5), 2.012 (5), and 2.028 (5) Å) and one apical Cu–N bond (2.210 (6) Å). The structure of **2** consists of discrete $[M(Me_4BIM)_2ONO_2]^+$ cations (M = Zn, Cu) separated by NO_3^- groups in a lattice not isostructural to that exhibited by **1**; no indications of disorder due to the Cu(II) dopant were detected. The Zn(II) coordination mainly differs from that of **1** in that no Zn–ligand bond is obviously apical. Electronic spectral and ESR spectral studies were performed on these complexes as well as those of the parent BIM ligand. Energies of the BIM and Me_4BIM molecular orbitals have been calculated by an INDO/S method. Of particular spectroscopic interest are the ligand orbitals of $\pi_1 - \pi_1$ and $\pi_1 + \pi_1$ character, where π_1 is the HOMO supplied by each imidazole fragment. Both $(\pi_1 - \pi_1) \rightarrow$ Cu(II) and $(\pi_1 + \pi_1) \rightarrow$ Cu(II) ligand to metal charge-transfer (LMCT) absorptions are exhibited by these complexes in the spectral region between the ligand field absorptions and the near-UV absorption edge resulting from ligand $\pi \rightarrow \pi^*$ transitions. These spectroscopic studies point to the unusual result that the Cu(II) chromophore present in **1** persists relatively unchanged in CH_3OH solution and in the lattice of the Zn(II) analogue, which exhibits a somewhat different coordination geometry.

Copper–imidazole ligation has been demonstrated for a wide variety of proteins including plastocyanin,[2] azurin,[3] superoxide dismutase,[4] serum albumin,[5] stellacyanin,[6] galactose oxidase,[7] cytochrome *c* oxidase,[8] ceruloplasmin,[9] hemocyanin,[10] and tyrosinase.[11] Because of their biological significance, numerous model imidazole-containing copper(II) chromophores have been the subjects of crystallographic and a wide variety of spectroscopic studies. We have been studying the LMCT absorptions of various Cu(II)–imidazole chromophores.[12,13] Plausible assignments have been proposed for the LMCT absorptions exhibited by easily synthesized tetragonal Cu(II)–imidazole chromophores. Electronically related Cu(II) protein chromophores such as those present in native and Cu(II)-doped superoxide dismutase are thought to exhibit LMCT absorptions at similar energies.[14] Considerably red-shifted LMCT spectra are expected for plastocyanin, azurin, stellacyanin, and other proteins that contain trigonally distorted[15] pseudotetrahedral Cu(II) chromophores having relatively small ligand fields.[16] The syntheses of model pseudotetrahedral Cu(II)–imidazole chromophores may facilitate the resolution of important electronic spectral,[15] vibrational,[17] and other questions regarding the protein binding sites. We decided to explore the use of sterically hindered rigid biimidazole ligands such as 4,4′,5,5′-tetramethyl-2,2′-biimidazole in an attempt to effect a tetrahedral distortion of the tetragonal coordination geometry commonly exhibited by the tetrakis Cu(II) complexes of simple imidazole ligands. Molecular models indicated that the 2:1 Cu(II) complexes of alkylated biimidazole ligands sterically were prevented from adopting approximately planar CuN_4 units. Precedent for this strategy has been established by the pseudotetrahedral CuN_4 coordination geometries reported for $Cu[(CH_3)_2Ga(3,5\text{-dimethylpyrazolate})_2]$[18] and several Cu(II) complexes of bis(2-pyridyl)amine ligands.[19] Recent studies of the 2:1 Cu(II) complexes of 4,4′,6,6′-tetramethyl-2,2′-bipyridyl[20] were conducted for similar reasons. Unfortunately, the 2:1 Cu(II) complexes of 2,2′-biimidazole and 2,2′-bipyridyl ligands crystallize as five-coordinate species. However, the five-coordinate geometries of the Cu(II) complexes of alkylated biimidazole ligands largely are retained both in methanolic solution and in solid solutions in the lattices of the structurally similar Zn(II) analogues. Cu(II)–imidazole chromophores which are both structurally defined *and magnetically dilute*

(1) (a) Rutgers University, New Brunswick. (b) Rutgers University, Newark.
(2) Colman, P. M.; Freeman, H. C.; Guss, J. M.; Murata, M.; Norris, V. A.; Ramshaw, J. A. M.; Venkatappa, M. P. *Nature (London)* **1978**, *272*, 319–24.
(3) Adman, E. T.; Steinkamp, R. E.; Sieker, L. C.; Jensen, L. H. *J. Mol. Biol.* **1978**, *123*, 35–47.
(4) Richardson, J. E.; Thomas, K. A.; Rubin, B. H.; Richardson, D. C. *Proc. Natl. Acad. Sci. U.S.A.* **1975**, *72*, 1349–53.
(5) Bradshaw, R. A.; Shearer, W. T.; Gurd, F. R. N. *J. Biol. Chem.* **1968**, *243*, 3817–25.
(6) Ulrich, E. L.; Markley, J. C. *Coord. Chem. Rev.* **1978**, *27*, 109–40.
(7) Bereman, R. D.; Kosman, D. J. *J. Am. Chem. Soc.* **1977**, *99*, 7322–5.
(8) Palmer, G.; Babcock, G. T.; Vickery, L. E. *Proc. Natl. Acad. Sci. U.S.A.* **1976**, *73*, 2206–10.
(9) Fee, J. A. *Struct. Bonding (Berlin)* **1975**, *23*, 1–60.
(10) Freedman, T. B.; Loehr, J. S.; Loehr, T. M. *J. Am. Chem. Soc.* **1976**, *98*, 2809–15.
(11) Himmelwright, R. S.; Eickman, N. C.; LuBien, C. D.; Lerch, K.; Solomon, E. I. *J. Am. Chem. Soc.* **1980**, *102*, 7339–44.
(12) Fawcett, T. G.; Bernarducci, E. E.; Krogh-Jespersen, K.; Schugar, H. J. *J. Am. Chem. Soc.* **1980**, *102*, 2598–604.
(13) Bernarducci, E.; Schwindinger, W. F.; Hughey, J. L.; Krogh-Jespersen, K.; Schugar, H. J. *J. Am. Chem. Soc.* **1981**, *103*, 1686–91.
(14) Pantoliano, M. W.; Valentine, J. S.; Nafie, L. A. *J. Am. Chem. Soc.* **1982**, *104*, 6310–7.
(15) Penfield, K. W.; Gay, R. R.; Himmelwright, R. S.; Eickman, N. C.; Norris, V. A.; Freeman, H. C.; Solomon, E. I. *J. Am. Chem. Soc.* **1981**, *103*, 4382–8.
(16) Solomon, E. I.; Hare, J. W.; Dooley, D. M.; Dawson, J. H.; Stephens, P. J.; Gray, H. B. *J. Am. Chem. Soc.* **1980**, *102*, 168–78.
(17) Gray, H. B.; Solomon, E. I. In "Copper Proteins"; Spiro, T. G., Ed.; Wiley: New York, 1981; Vol. 3, Chapter 1.
(18) Patmore, D. J.; Rendle, D. F.; Storr, A.; Trotter, J. *J. Chem. Soc., Dalton Trans.* **1975**, 718–25.
(19) Gouge, E. M.; Geldard, J. F.; Sinn, E. *Inorg. Chem.* **1980**, *19*, 3356–9.
(20) Burke, P. J.; Henrick, K.; McMillin, D. R. *Inorg. Chem.* **1982**, *21*, 1881–6.

0020-1669/83/1322-3911$01.50/0

are promising candidates for ESR spin-echo studies. Such studies have revealed interesting nuclear modulation patterns between the Cu(II) spin and the "remote" nitrogen atom of the imidazole ligation;[21] they should be even more revealing for structurally unambiguous Cu(II)–imidazole chromophores.

We report here the preparation and characterization of complexes **1**–**6**. The structures of **1** and **2** have been determined by X-ray crystallographic studies. Electronic spectral and ESR studies have been performed on the neat complexes **1**–**6** as well as on methanolic solutions of **1**, **3**, and **5**. Finally, the electronic structures of the free biimidazole ligands have been probed by MO calculations and correlated with the electronic structures of imidazole and 4,5-dialkylated imidazoles. These results have facilitated the assignment of the LMCT absorptions exhibited by these Cu(II)–biimidazole chromophores.

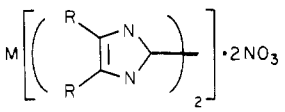

1: M = Cu(II), R = CH_3
2: M = $Cu(II)_{0.1}Zn(II)_{0.9}$, R = CH_3
3: M = Cu(II), R–R = $-CH_2CH_2CH_2CH_2-$
4: M = $Cu(II)_{0.1}Zn(II)_{0.9}$, R–R = $-CH_2CH_2CH_2CH_2-$
5: M = Cu(II), R = H
6: M = $Cu(II)_{0.1}Zn(II)_{0.9}$, R = H

Experimental Section

Preparation of 2,2′-Biimidazole (BIM). In accordance with a published procedure,[22] a slurry of glyoxal bisulfite (50 g),[23] $(NH_4)_2CO_3$ (10 g), and 250 mL of concentrated aqueous NH_3 was heated on a steam bath for 2 h. During that time, the glyoxal bisulfite dissolved, the solution changed from colorless to dark brown, and tan needles of the product formed. The crude product was collected by filtration, washed with water and acetone, and dried in air (yield 2.5 g, 44% based on glyoxal). The product was dissolved in 150 mL of boiling ethylene glycol and decolorized with 1 g of charcoal. The cooled filtrate (268 K) deposited white needles, which were collected, washed, and dried as described above (yield 2 g, 35%): mp >590 K; ^1H NMR (10% DCl, 60 MHz) δ 7.6 (s, ArH).

Preparation of 4,4′,5,5′-Tetramethyl-2,2′-biimidazole (Me_4BIM). In accordance with a published procedure,[24] a slurry of glyoxal bisulfite (15.7 g),[23] $(NH_4)_2CO_3$ (10 g), 2,3-butanedione (9 mL), and 150 mL of concentrated aqueous NH_3 was heated on a steam bath for 3 h. The crude product separated from the dark brown reaction mixture as tan needles and was collected and purified in the manner described above for BIM (yield 0.9 g, 12%): mp >610 K; ^1H NMR (10% DCl, 60 MHz) δ 2.4 (s, CH_3). The infrared spectra of Me_4BIM agreed with those published by Aldrich.[25]

Preparation of 4,4′,5,5′,6,6′,7,7′-Octahydro-2,2′-bibenzimidazole (BIBENZ). A stirred and warmed (313 K) solution of 1,2-cyclohexanedione (5.5 g) and 40% aqueous glyoxal (3.7 g) in 100 mL of ethanol was saturated with dry ammonia gas. After 30 min, the resulting tan solid was separated from the yellow solution and collected and purified as described above. The purified product (white needles) was obtained in 8% overall yield: mp >615 K; ^1H NMR (10% DCl, 60 MHz) δ 2.8 (m, CH_2, 8 H), 2.0 (m, CH_2, 8 H). The infrared spectra of the product (KBr pellet) were similar in appearance to those observed for Me_4BIM. In particular, the absorptions of the product at 1600 (s), 1440 (m), 1380 (s), 1250 (w), 1195 (s), 951 (m), and 939 (w) cm^{-1} also were exhibited by Me_4BIM. Anal. Calcd for $C_{14}H_{18}N_4$: C, 69.39; H, 7.43; N, 23.12. Found: C, 68.57; H, 7.54; N, 23.44.

Preparation of Me_4BIM Complexes 1 and 2. Complex **1** was prepared by the addition of 0.063 g (0.26 mmol) of $Cu(NO_3)_2 \cdot 3H_2O$ to a slurry of 0.1 g (0.52 mmol) of Me_4BIM in 20 mL of methanol. The resulting reddish purple solution was filtered and evaporated in air at room temperature. The solution deposited well-formed red-purple crystals (rectangular prisms), which were collected by filtration and dried in air. The measured density (flotation in cyclohexane/ethylene dibromide) of these air-stable crystals was 1.45 (1) g/mL. Anal. Calcd for $CuC_{20}H_{28}N_{10}O_6$: Cu, 11.17; C, 42.29; H, 5.37; N, 24.46. Found: Cu, 11.35; C, 42.20; H, 5.01; N, 24.56.

The Cu(II)-doped complex **2** was prepared by adding 0.07 g (0.23 mmol) of $Zn(NO_3)_2 \cdot 6H_2O$ and 0.006 g (0.024 mmol) of $Cu(NO_3)_2 \cdot 3H_2O$ to a slurry of 0.1 g (0.52 mmol) of the ligand in 5 mL of methanol. The resulting pale purple solution was filtered and evaporated in air at room temperature. The solution deposited pale red-purple crystals (rectangular prisms), which were collected by filtration and dried. The density of these air-stable crystals was 1.43 (1) g/mL. Microscopic examination suggested that the crystals were homogeneous and uniformly doped with copper. Assays of copper and zinc by atomic absorption spectroscopy revealed that the composition of **2** was $Cu^{II}_{0.1}Zn^{II}_{0.9}[Me_4BIM]_2 \cdot 2NO_3$. X-ray powder diffraction studies showed that complexes **1** and **2** were not isomorphous.

Preparation of BIBENZ Complexes 3 and 4. Complex **3** was prepared from $Cu(NO_3)_2 \cdot 3H_2O$ and BIBENZ in a manner analogous to that described above for **1** and was isolated as red-brown prisms. The density of these air-stable crystals was 1.42 (1) g/mL. Anal. Calcd for $CuC_{28}H_{36}N_{10}O_6 \cdot CH_3OH$: Cu, 9.02; C, 49.46; H, 5.72; N, 19.89. Found: Cu, 9.34; C, 48.47; H, 5.55; N, 19.66.

Complex **4**, doped at approximately the 10% level, was prepared in a manner similar to that described for **2** and was isolated as pale red-brown prisms. The density of these air-stable crystals was 1.41 (1) g/mL.

Preparation of BIM Complexes 5 and 6. The BIM complexes of Cu(II) and Zn(II) were less soluble in methanol than those of Me_4BIM and BIBENZ. Complex **5** was prepared by the addition of 0.09 g (0.37 mmol) of $Cu(NO_3)_2 \cdot 3H_2O$ to a slurry of 0.1 g (0.77 mmol) of BIM in 10 mL of methanol. The resulting green solution rapidly deposited a powdery green solid, which was collected by filtration and recrystallized from ~30 mL of hot methanol. The methanol solution deposited well-formed green plates, which were collected by filtration and dried. The density of these air-stable crystals was 1.76 (1) g/mL. A perchlorate analogue of **5**, $Cu(BIM)_2 \cdot 2ClO_4$, has been prepared and characterized by other workers.[26] Anal. Calcd for $CuC_{12}H_{12}N_{10}O_6$: Cu, 13.93; C, 31.62; H, 2.65; N, 30.72. Found: Cu, 13.78; C, 31.72; H, 2.66; N, 30.71.

Complex **6** was prepared by the addition of 0.2 g (0.67 mmol) of $Zn(NO_3)_2 \cdot 6H_2O$ and 0.018 g (0.07 mmol) of $Cu(NO_3)_2 \cdot 3H_2O$ to a slurry of 0.2 g (1.5 mmol) of BIM in 20 mL of methanol. A pale green powder rapidly precipitated from the resulting pale green solution. The precipitate was collected by filtration and recrystallized from ~60 mL of hot methanol. The methanol solution deposited pale green plates, which became opaque when exposed to air. It was possible to determine the density of complex **6** (1.76 (1) g/mL, cyclohexane/ethylene dibromide) before the crystals turned opaque.

X-ray Diffraction Studies. Crystals of **1** and **2** were mounted along their *a* axes on glass fibers. Crystal data and additional details of the data collection and refinement are presented in Table I. Intensity data were collected and corrected for decay, Lp effects, and absorption as described previously.[27] Standard deviations were assigned as $\sigma(F^2) = (Lp)^{-1}[N_t + (0.03N_n)^2]^{1/2}$, where N_t is the total count and N_n is the net count. Diffractometer examination of the reciprocal lattices of both complexes revealed no systematic absences.

The structure of **1** was solved by direct methods[28] and refined successfully in space group $P\bar{1}$ with use of full-matrix least-squares techniques. Neutral-atom scattering factors[29] were used, and anom-

(21) Mims, W. B.; Peisach, J. *Biochemistry* **1976**, *15*, 3863–8.
(22) Holmes, F.; Jones, K. M.; Torrible, E. G. *J. Chem. Soc.* **1961**, 4790–5.
(23) Horning, E. C. "Organic Syntheses"; Wiley: New York, 1955; Collect. Vol. III, p 438.
(24) Kuhn, R.; Blau, W. *Justus Liebigs Ann. Chem.* **1957**, *605*, 32–5.
(25) Pouchert, C. J. "Aldrich Library of Infrared Spectra", 3rd ed.; Aldrich Chemical Co.: Milwaukee, 1981; p 1218.
(26) Sakaguchi, U.; Addison, A. W. *J. Chem. Soc., Dalton Trans.* **1979**, 600–8.
(27) Hughey, J. L.; Fawcett, T. G.; Rudich, S. M.; Lalancette, R. A.; Potenza, J. A.; Schugar, H. J. *J. Am. Chem. Soc.* **1979**, *101*, 2617–23.
(28) In addition to local programs for the IBM 370/168 computer, local modifications of the following programs were employed: Coppens' ABSORB program; Zalkin's FORDAP Fourier program; Johnson's ORTEP II thermal ellipsoid plotting program; Busing, Martin, and Levy's ORFEE error function program; Main, Lessinger, Declercq, Woolfson, and Germain's MULTAN 78 program for the automatic solution of crystal structures; the FLINUS least-squares program obtained from Brookhaven National Laboratories.
(29) Cromer, D. T.; Waber, J. T. *Acta Crystallogr.* **1965**, *18*, 104–9.

Table I. Crystal and Refinement Data for **1** and **2**

	$CuC_{20}H_{28}N_{10}O_6$	$Zn_{0.9}Cu_{0.1}C_{20}H_{28}N_{10}O_6$
fw	567.93	569.70
a, Å	7.854 (1)	7.812 (1)
b, Å	14.303 (2)	13.324 (3)
c, Å	11.852 (2)	13.692 (3)
α, deg	78.46 (2)	72.72 (2)
β, deg	94.96 (2)	107.00 (1)
γ, deg	91.92 (1)	96.77 (1)
space group	$P\bar{1}$	$P\bar{1}$
Z	2	2
no. of reflcns used to determine cell constants	15	13
d_{calcd}, g/cm³	1.451	1.454
d_{obsd}, g/cm³	1.45 (1)[a]	1.43 (1)[a]
λ(Mo Kα), Å	0.710 69	0.710 69
monochromator	graphite	graphite
linear abs coeff, cm⁻¹	9.31	9.65
cryst dimens, mm	0.43 × 0.32 × 0.10	0.47 × 0.17 × 0.08
abs factor range	1.14–1.41	1.05–1.19
diffractometer	Syntex $P2_1$	Syntex $P2_1$
data collection method	θ–2θ	θ–2θ
2θ range, deg	3–50	3–50
temp, K	303 ± 1	298 ± 1
scan rate, deg/min	2.5[b]	2.5[b]
scan range, deg	2θ(Kα₁) − 1 to 2θ(Kα₁) + 1	2θ(Kα₁) − 1 to 2θ(Kα₁) + 1
no. of std reflcns	3	3
% variation in std intens	±4	±5
no. of unique data collected	4591	4612
no. of data used in refinement ($F_o^2 \geq 2\sigma(F_o^2)$)	2138	2391
data:parameter ratio	6.4	7.1
final R_F[c]	0.057	0.056
final R_{wF}[d]	0.048	0.047

[a] Determined by flotation in mixtures of cyclohexane and 1,2-dibromoethane. [b] Stationary background counts were taken before and after the scan. The total time for background counting was equal to the scan time and was distributed equally before and after the peak. [c] $R_F = \Sigma ||F_o| - |F_c|| / \Sigma |F_o|$. [d] $R_{wF} = (\Sigma w(|F_o| - |F_c|)^2 / \Sigma w F_o^2)^{1/2}$.

alous dispersion corrections[30] were applied to the Cu and Cl atoms. An *E* map, based on 300 phases from the starting set with the highest combined figure of merit, revealed the Cu and N atoms, along with portions of the ligands. The remaining non-hydrogen atoms were located on subsequent difference Fourier maps. Several cycles of isotropic refinement led to convergence with $R_F = 0.117$.

Hydrogen atoms were added to the model at calculated positions with N–H bond lengths taken to be 0.87 Å.[37] A planar geometry was assumed for the aromatic N atoms, while methyl C atoms were assumed to be tetrahedral with C–H bond lengths of 0.95 Å.[31] Methyl H atoms were located by rotating at 5° intervals the idealized tetrahedral positions and computing the electron densities at these positions. The orientation with the highest combined electron density was used. H atoms were assigned temperature factors according to $B_H = B_N + 1$, where N is the atom bonded to H. Hydrogen atom parameters were not refined. Additional refinement, using anisotropic thermal parameters for all non-hydrogen atoms, reduced R_F to 0.057 and R_{wF} to 0.048. For the final cycle, all parameter changes were within 0.4σ, where σ is the esd obtained from the inverse matrix. A final difference map showed a general background of approximately ±0.4 e/Å³. The largest peak (0.65 e/Å³) was located near atom O(3). Final atomic parameters are listed in Table II while a view of the complex is given in Figure 1.

The structure of **2** was solved and refined in space group $P\bar{1}$ in a similar fashion with the metal center assumed to be entirely zinc.

(30) "International Tables for X-ray Crystallography"; Kynoch Press: Birmingham, England, 1962; Vol. III, pp 201–13.
(31) Churchill, M. R. *Inorg. Chem.* **1973**, *12*, 1213–4.

Table II. Fractional Atomic Coordinates and Thermal Parameters for **1** and **2**[a,b]

	x	*y*	*z*	B_{eq}, Å²
Cu	0.0538 (1)	0.35345 (7)	0.77551 (9)	4.42 (3)
Zn	0.8993 (1)	0.27928 (7)	0.85228 (7)	4.09 (3)
N(1)	−0.0496 (7)	0.2929 (4)	0.9428 (5)	4.3 (2)
	0.9716 (7)	0.1701 (4)	0.7920 (5)	3.9 (2)
N(2)	−0.2055 (7)	0.3296 (4)	1.0724 (5)	4.3 (2)
	1.1294 (6)	0.0299 (4)	0.8299 (4)	4.0 (2)
N(3)	−0.2210 (6)	0.5326 (4)	0.9086 (5)	4.1 (2)
	1.2602 (7)	0.0598 (4)	1.0627 (4)	4.0 (2)
N(4)	−0.0823 (7)	0.4656 (4)	0.7933 (5)	4.2 (2)
	1.0985 (7)	0.2013 (4)	0.9907 (4)	4.0 (2)
N(5)	0.1944 (7)	0.2444 (4)	0.7599 (5)	4.2 (2)
	0.6777 (7)	0.3587 (4)	0.7383 (4)	3.6 (2)
N(6)	0.2158 (7)	0.1177 (4)	0.6826 (4)	4.1 (2)
	0.5761 (8)	0.5157 (4)	0.6432 (4)	4.1 (2)
N(7)	−0.1620 (7)	0.1822 (4)	0.5681 (4)	4.0 (2)
	0.9822 (7)	0.5904 (4)	0.7121 (4)	3.9 (2)
N(8)	−0.1049 (7)	0.3029 (4)	0.6563 (4)	3.6 (2)
	1.0205 (7)	0.4256 (4)	0.8119 (4)	3.7 (2)
C(1)	−0.0687 (10)	0.2130 (5)	1.0295 (7)	4.7 (2)
	0.9435 (9)	0.1389 (5)	0.7000 (5)	3.8 (2)
C(2)	−0.1621 (10)	0.2353 (5)	1.1093 (6)	4.5 (2)
	1.0373 (9)	0.0515 (6)	0.7222 (6)	4.1 (2)
C(3)	−0.1377 (8)	0.3609 (5)	0.9707 (6)	3.8 (2)
	1.0859 (8)	0.1030 (5)	0.8675 (5)	3.4 (2)
C(4)	−0.1473 (8)	0.4525 (5)	0.8941 (6)	3.6 (2)
	1.1492 (8)	0.1186 (5)	0.9724 (5)	3.4 (2)
C(5)	−0.2010 (8)	0.6009 (5)	0.8122 (7)	3.8 (2)
	1.2820 (8)	0.1092 (5)	1.1425 (5)	3.9 (2)
C(6)	−0.1159 (9)	0.5597 (5)	0.7399 (6)	4.2 (2)
	1.1797 (9)	0.1952 (5)	1.0959 (6)	4.1 (2)
C(7)	0.0093 (11)	0.1199 (5)	1.0263 (7)	7.4 (3)
	0.8232 (10)	0.1975 (6)	0.5964 (6)	5.9 (3)
C(8)	−0.2172 (10)	0.1796 (6)	1.2214 (7)	6.9 (3)
	1.0528 (10)	−0.0143 (6)	0.6541 (5)	5.9 (3)
C(9)	−0.2726 (9)	0.6995 (5)	0.7998 (6)	5.5 (2)
	1.4023 (9)	0.0679 (5)	1.2508 (5)	5.4 (3)
C(10)	−0.0643 (10)	0.6021 (5)	0.6221 (7)	6.6 (3)
	1.1555 (10)	0.2777 (6)	1.1448 (6)	6.4 (3)
C(11)	0.3476 (9)	0.2001 (5)	0.8016 (6)	4.4 (2)
	0.4963 (9)	0.3483 (5)	0.6936 (5)	3.9 (2)
C(12)	0.3620 (9)	0.1224 (5)	0.7548 (6)	4.3 (2)
	0.4323 (9)	0.4441 (6)	0.6338 (5)	4.0 (2)
C(13)	0.1200 (8)	0.1918 (5)	0.6888 (5)	3.5 (2)
	0.7206 (9)	0.4603 (6)	0.7068 (5)	3.5 (2)
C(14)	−0.0467 (8)	0.2234 (5)	0.6334 (5)	3.5 (2)
	0.9046 (9)	0.4960 (5)	0.7407 (5)	3.6 (2)
C(15)	−0.3037 (8)	0.2400 (5)	0.5460 (5)	3.9 (2)
	1.1632 (10)	0.5809 (6)	0.7667 (6)	4.3 (3)
C(16)	−0.2672 (9)	0.3138 (5)	0.6006 (6)	4.2 (2)
	1.1847 (9)	0.4795 (6)	0.8264 (5)	3.8 (2)
C(17)	0.4715 (10)	0.2345 (6)	0.8896 (7)	7.4 (3)
	0.3998 (9)	0.2439 (6)	0.7116 (6)	5.7 (3)
C(18)	0.5023 (10)	0.0510 (5)	0.7681 (7)	7.0 (3)
	0.2466 (9)	0.4770 (6)	0.5695 (5)	5.4 (3)
C(19)	−0.4592 (10)	0.2147 (6)	0.4744 (7)	7.0 (3)
	1.2914 (10)	0.6737 (6)	0.7527 (6)	6.2 (3)
C(20)	−0.3798 (9)	0.3968 (5)	0.5997 (7)	6.2 (3)
	1.3528 (9)	0.4263 (6)	0.8991 (6)	3.4 (2)
N(9)	0.3182 (10)	0.4930 (6)	0.7834 (10)	7.3 (3)
	0.7013 (8)	0.2037 (6)	0.9977 (6)	5.1 (2)
O(1)	0.2606 (9)	0.4261 (5)	0.8605 (6)	9.0 (3)
	0.7145 (6)	0.1564 (4)	0.9332 (4)	5.9 (2)
O(2)	0.2789 (10)	0.4753 (6)	0.6894 (6)	10.4 (3)
	0.7485 (7)	0.2979 (4)	0.9835 (4)	6.4 (2)
O(3)	0.3919 (9)	0.5544 (6)	0.8100 (10)	16.4 (5)
	0.6492 (7)	0.1547 (4)	1.0755 (5)	8.0 (2)
N(10)	0.1581 (8)	0.0582 (5)	0.4206 (6)	5.1 (2)
	0.6859 (10)	0.7937 (6)	0.5428 (5)	5.4 (3)
O(4)	0.1293 (6)	0.1417 (3)	0.4269 (4)	5.8 (2)
	0.5785 (7)	0.7299 (4)	0.5823 (4)	7.3 (2)
O(5)	0.1373 (8)	0.0305 (4)	0.3286 (5)	8.0 (2)
	0.6442 (7)	0.8842 (4)	0.4943 (5)	7.9 (2)
O(6)	0.2004 (6)	−0.0020 (3)	0.5123 (4)	5.1 (5)
	0.8384 (8)	0.7643 (4)	0.5543 (4)	7.6 (2)

[a] $B_{eq} = 8\pi^2/3(U_{11}a^{*2}a^2 + U_{12}a^*b^*ab\cos\gamma + \ldots)$. [b] Parameters for the Cu-doped structure **2** are given below those for **1**.

Table III. Selected Bond Distances (Å) and Angles (deg) in **1** and **2**[a]

		Coordination Sphere	
Cu[Zn]-N(4)	2.012 (5) [2.103 (5)]	Cu[Zn]-N(8)	2.028 (5) [2.058 (5)]
Cu[Zn]-N(5)	1.987 (5) [2.103 (5)]	Cu[Zn]-N(1)	2.210 (6) [2.072 (5)]
Cu[Zn]-O(1)	2.180 (7) [2.300 (5)]	Cu[Zn]-O(2)*	2.569 (8) [2.499 (5)]
		Ligands and Counterion	
C(14)-N(8)	1.326 (7) [1.337 (7)]	C(4)-N(4)	1.316 (7) [1.325 (7)]
C(14)-N(7)	1.338 (7) [1.330 (7)]	C(4)-N(3)	1.348 (7) [1.360 (7)]
C(13)-N(5)	1.325 (7) [1.326 (7)]	C(3)-N(1)	1.322 (7) [1.328 (7)]
C(13)-N(6)	1.337 (7) [1.348 (7)]	C(3)-N(2)	1.348 (7) [1.343 (7)]
N(8)-C(16)	1.382 (8) [1.385 (7)]	N(4)-C(6)	1.391 (7) [1.375 (7)]
N(5)-C(11)	1.384 (7) [1.377 (7)]	N(1)-C(1)	1.389 (8) [1.391 (8)]
C(16)-C(15)	1.354 (8) [1.356 (8)]	C(5)-C(6)	1.362 (8) [1.357 (8)]
C(11)-C(12)	1.349 (8) [1.356 (8)]	C(1)-C(2)	1.337 (9) [1.358 (8)]
C(15)-N(7)	1.384 (7) [1.393 (7)]	C(5)-N(3)	1.363 (8) [1.395 (7)]
C(12)-N(6)	1.379 (7) [1.387 (7)]	C(2)-N(2)	1.376 (8) [1.396 (8)]
C(16)-C(20)	1.520 (9) [1.501 (8)]	C(6)-C(10)	1.491 (9) [1.501 (9)]
C(15)-C(19)	1.501 (9) [1.498 (8)]	C(5)-C(9)	1.510 (9) [1.486 (8)]
C(11)-C(17)	1.508 (9) [1.491 (9)]	C(1)-C(7)	1.493 (9) [1.496 (9)]
C(12)-C(18)	1.504 (9) [1.498 (8)]	C(2)-C(8)	1.496 (9) [1.494 (9)]
C(13)-C(14)	1.456 (8) [1.445 (8)]	C(3)-C(4)	1.437 (9) [1.445 (9)]
		Ligand NO_3^-	
N(9)-O(1)	1.285 (9) [1.254 (7)]	N(9)-O(3)	1.118 (8) [1.227 (7)]
N(9)-O(2)	1.202 (9) [1.240 (7)]		
		Lattice NO_3^-	
N(10)-O(4)	1.240 (7) [1.242 (7)]	N(10)-O(6)	1.271 (7) [1.249 (7)]
N(10)-O(5)	1.229 (7) [1.220 (7)]		
		Coordination Sphere	
N(4)-Cu[Zn]-N(1)	80.8 (2) [81.4 (2)]	N(4)-Cu[Zn]-O(1)	83.2 (2) [81.7 (2)]
N(5)-Cu[Zn]-O(1)	95.1 (3) [91.3 (2)]	N(4)-Cu[Zn]-N(8)	99.5 (2) [101.0 (2)]
N(5)-Cu[Zn]-N(8)	88.1 (2) [81.5 (2)]	O(1)-Cu[Zn]-O(2)*	49.6 (2) [53.1 (2)]
N(5)-Cu[Zn]-N(1)	99.3 (2) [108.0 (2)]	N(1)-Cu[Zn]-O(2)*	140.4 (2) [143.1 (2)]
N(8)-Cu[Zn]-O(1)	163.8 (2) [154.9 (2)]	N(4)-Cu[Zn]-O(2)*	86.9 (2) [84.1 (2)]
N(1)-Cu[Zn]-O(1)	91.4 (2) [91.2 (2)]	N(5)-Cu[Zn]-O(2)*	91.9 (2) [84.3 (2)]
N(8)-Cu[Zn]-N(1)	104.8 (2) [114.0 (2)]	N(8)-Cu[Zn]-O(2)*	114.3 (2) [101.9 (2)]
N(4)-Cu[Zn]-N(5)	178.3 (4) [168.5 (2)]		
		Possible Hydrogen-Bonding Interactions	
O(4)···N(6)	3.002 (8) [2.725 (8)]	O(6)···N(6)	2.890 (7) [-]
O(4)···N(7)	3.084 (7) [-]	O(6)···N(7)	- [2.742 (8)]
O(4)···H-N(6)	114.5 [167.6]	O(6)···H-N(6)	160.2 [-]
O(4)···H-N(7)	109.5 [-]	O(6)···H-N(7)	- [168.6]

[a] The corresponding structural parameters determined for **1** and **2** (bracketed numbers) are presented side by side.

Following the location of all non-hydrogen atoms, isotropic refinement converged with $R_F = 0.121$. After the addition of hydrogen atoms, anisotropic refinement converged with $R_F = 0.056$ and $R_{wF} = 0.047$, values which are slightly lower than those observed for **1**. For the final refinement cycle, all parameter changes were within 0.3σ. A final difference map showed a general background of approximately ±0.3 e/Å^3. The largest residual (0.53 e/Å^3) was located 1.25 Å from the zinc atom and may be related to the presence of copper in the structure. However, the size of this residual precludes any substantial disorder at the metal site. Final atomic parameters are listed in Table II. Lists of observed and calculated structure factors, anisotropic thermal parameters, and calculated hydrogen atom parameters are available for both structures.[32]

Details of the Calculations. MO calculations for BIM and Me_4BIM as well as for the reference monomeric imidazole and 4,5-dimethylimidazole molecules were performed with use of a semiempirical all valence electron INDO/S method.[33] Values for the one-center, two-electron integrals γ_{AA} were taken from Del Bene and Jaffé.[34] Two-center, two-electron integrals γ_{AB} were evaluated with the interpolation formula proposed by Mataga and Nishimoto.[35] The atomic parameters β^0_A are those of Ellis, Kuehnlenz, and Jaffé[36] with π-screening constants $K_{CC} = 0.570$, $K_{CN} = K_{NN} = 0.585$. Bond distances and angles of the BIM and Me_4BIM ligands were based upon the geometries crystallographically determined for the $Ni(BIM)_2(NO_3)_2 \cdot 2H_2O$ complex[37] and complexes **1** and **2**. Structural parameters of imidazole were taken from a published crystallographic study.[38] The electronically excited states were calculated in the singly excited configuration interaction approximation with all configurations of (n, π^*) and (π,π^*) types included; oscillator strengths were determined with the dipole length operator. The calculated orbital and transition energies are relatively insensitive to small changes in the atomic parameters or molecular geometries employed.

Physical Measurements. Electronic spectra were recorded with a Cary Model 17 R1 spectrophotometer. Presentation of the data on linear energy scales was facilitated by a Tektronix Model 4052 computer/plotter system. ESR spectra were measured with a Varian Model E-12 spectrometer calibrated with a Hewlett-Packard Model 5245L frequency counter and a DPPH crystal ($g = 2.0036$).

Results and Discussion

Description of the Structures. Selected bond distances and angles for **1** and **2** are given in Table III. The structure of **1** (Figure 1) consists of discrete $[Cu(Me_4BIM)_2ONO_2]^+$ cations separated by lattice NO_3^- groups. The copper atom exhibits N_4OO^* coordination resulting from bidentate ligation by two Me_4BIM molecules and anisobidentate ligation by a

(32) Supplementary material.
(33) Krogh-Jespersen, K.; Ratner, M. A. *Theor. Chim. Acta*, **1978**, *47*, 283–96.
(34) Del Bene, J.; Jaffé, H. H. *J. Chem. Phys.* **1968**, *48*, 1807–13.
(35) Mataga, N.; Nishimoto, K. *Z. Phys. Chem. (Wiesbaden)* **1957**, *13*, 140–57.
(36) Ellis, R. L.; Kuehnlenz, G.; Jaffé, H. H. *Theor. Chim. Acta* **1972**, *26*, 131–40.
(37) Mighell, A. D.; Reimann, C. W.; Mauer, F. A. *Acta Crystallogr., Sect. B: Struct. Crystallogr. Cryst. Chem.* **1969**, *B25*, 60–6.
(38) Fransson, G.; Lundberg, B. K. S. *Acta Chem. Scand.* **1972**, *26*, 3969–76.

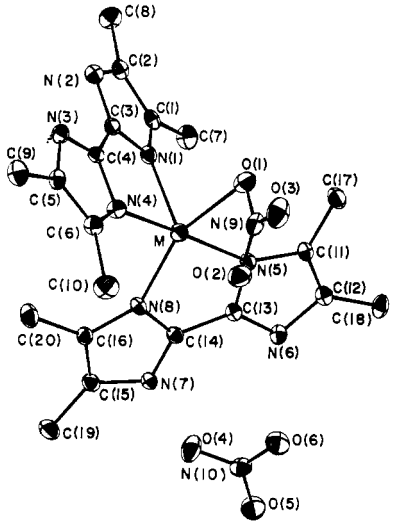

Figure 1. ORTEP view of complex **1** showing the atom-numbering scheme. Since the ORTEP views of complexes **1** and **2** nearly are identical, only a single view has been presented with M(II) = Cu(II) for complex **1** and M(II) = $Zn^{II}_{0.90}Cu^{II}_{0.10}$ for complex **2**.

NO_3^- group. Coordination by the NO_3^- group consists of a normal-length Cu–O(1) bond (2.180 (7) Å) along with an elongated Cu–O(2)* semibond (2.569 (8) Å). The general structural features observed for **1** closely correspond to those reported for $[Cu(bpy)_2ONO]BF_4$.[39] If the semibond is ignored, the distorted coordination geometry lies closer to the idealized square pyramid than to the idealized trigonal bipyramid. We interpret the greater length of the Cu–N(1) bond relative to those of the remaining three Cu–N bonds as indicating an apical interaction. In harmony with this view is the observation that bond angles between the apical N(1)–Cu bond and the O(1), N(4), N(5), N(8) equatorial ligation span the range 80.8 (2)–104.8 (2)° (the ideal value is 90°). Moreover, the N(4)–Cu–N(5) and N(8)–Cu–O(1) bond angles are appropriate for approximately trans equatorial ligation. This equatorial ligation exhibits a tetrahedral distortion with N(8) and O(1) lying on average ~0.14 Å below and N(4) and N(5) lying ~0.14 Å above the best plane defined by these donor atoms.[32] Also indicative of approximately square-pyramidal coordination is the displacement of copper by 0.15 Å from the best plane defined by N(8), O(1), N(4), and N(5) toward the apical N(1) donor atom. It appears less appropriate to view the coordination geometry of **1** as approximately trigonal bipyramidal. Although the CuN(1)O(1)N(8) unit is planar within experimental error, the bond angles within this unit are distorted significantly from the ideal value of 120°, with the largest differences observed for the O(1)–Cu–N(8) and O(1)–Cu–N(1) angles. Finally, the ESR spectra exhibited by methanolic **1** and polycrystalline **2** (see below) are those of tetragonal rather than trigonal-bipyramidal chromophores and suggest a $d_{x^2-y^2}$ ground state.

The crystallographic nonequivalence of the two Me_4BIM ligands is not reflected in the observed bond distances and angles. Inspection of Table III reveals that nearly all of the corresponding Me_4BIM structural parameters are equivalent within experimental error. Each imidazole ring is planar to ±0.01 Å. Moreover, the individual imidazole rings of each Me_4BIM ligand show only small deviations from coplanarity; the maximum displacement of any ring atom from the Me_4BIM planes is less than 0.08 Å, and the dihedral angles between the imidazole rings of a given ligand are less than 13°. The crystallographic nonequivalency of the Me_4BIM ligands resides primarily in their orientation. Relative to the N(4)–N(5)N(8)O(1) basal plane, the Me_4BIM ligand containing donor atoms N(5) and N(8) exhibits a dihedral angle of 2.9° whereas the Me_4BIM ligand containing N(1) and N(4) exhibits an angle of 97.7°. Finally, the observed bond distances and angles within the biimidazole ligands compare well with those reported for other structures containing imidazole ligands.[40]

Both NO_3^- groups nearly are triangular. Bond distances for the bound nitrate span an unusually large range (1.118 (8)–1.285 (9) Å). The relatively short N(9)–O(2) and N(9)–O(3) distances may be related to the large thermal parameters for these atoms. The lattice nitrate in **1** as well as both nitrate groups in **2** exhibit considerably smaller thermal parameters and much more uniform bond distances, which compare favorably with those from other nitrate-containing structures.[41] The lattice NO_3^- group ($Cu\cdots ONO_2^- > 4$ Å) is held in the lattice by coulombic forces and by hydrogen bonds to imidazole N–H groups (Table III).

The rather similar structure of **2** consists of discrete $[Zn_{0.9}Cu_{0.10}(Me_4BIM)_2ONO_2]^+$ cations separated by lattice NO_3^- groups ($M(II)\cdots ONO_2^- > 4$ Å). Coordination by the NO_3^- group consists of a normal-length Zn–O(1) bond (2.300 (5) Å) along with an elongated Zn–O(2)* semibond (2.499 (5) Å). If the semibond is ignored, the distorted coordination geometry closely corresponds to that reported for $[Cu(bpy)_2ONO]BF_4$.[39] In contrast to the case for **1**, the structure of **2** lies somewhat closer to the idealized trigonal bipyramid, although it is still best described as a distorted square pyramid. Whereas the Cu–N(1) distance in **1** was relatively long and clearly appropriate for apical bonding, the corresponding Zn–N(1) distance is relatively short and comparable to the other Zn–N bond distances. The Zn, N(1), N(8), and O(1) atoms are coplanar to ±0.001 Å, but the associated bond angles (114.0 (2), 91.2 (2), 154.9 (2)°) deviate greatly from the ideal trigonal-bipyramidal value of 120°. However, the extent of this distortion is less than that exhibited by **1**. The observed metal–ligand bond distances and angles are unremarkable and agree with those reported for analogous Zn(II) complexes.[39] Structural parameters for the Me_4BIM ligands, coordinated NO_3^-, and lattice NO_3^- are similar to those for **1**.

Electronic Structure of Biimidazole Ligands. We begin with a brief review of the ligand $\pi \rightarrow \pi^*$ absorptions and ligand $\rightarrow$ Cu(II) LMCT absorptions for free and complexed imidazoles and then extend these results to the corresponding biimidazole ligands and complexes. Discussions of the spectroscopically relevant MO's of imidazole and alkylated imidazoles have been presented elsewhere.[13,40] Briefly, both the measured photoelectron spectra and various MO calculations yield the result that the three highest energy filled MO's of imidazole and alkylated imidazoles are well removed (>3 eV) from the more stable corelike orbitals. The HOMO is a ring orbital of π symmetry (π_1), which primarily has carbon 2p(π) character. A second, lower lying π orbital (π_2), which primarily has nitrogen 2p(π) character, and the n orbital, which consists primarily of the lone pair (σ symmetry) on the sp^2-type nitrogen donor atom, are close to each other in energy. Our INDO/S calculations indicate that dimethylation of imidazole at the 4- and 5-carbon atoms of the ring raises the energies of the π_2, n, π_1, π_1^* (LUMO), and π_2^* orbitals by approximately 0.3, 0.3, 0.6, 0.1, and 0.1 eV, respectively. Qualitatively, the greater destabilization of the π_1 orbital results from its substantial carbon 2p(π) character and the electron-donating property of methyl groups. Consequently, both the

(39) Walsh, A.; Walsh, B.; Murphy, B.; Hathaway, B. J. *Acta Crystallogr., Sect. B: Struct. Crystallogr. Cryst. Chem.* **1981**, *B37*, 1512–20.

(40) Bernarducci, E.; Bharadwaj, P. K.; Krogh-Jespersen, K.; Potenza, J. A.; Schugar, H. J. *J. Am. Chem. Soc.* **1983**, *105*, 3860–6.

(41) Nakai, H. *Bull. Chem. Soc. Jpn.* **1980**, *53*, 1321–6.

Table IV. Calculated Orbital and Excited State Energies (eV) for Imidazoles and Biimidazoles

	π_2	n	π_1	π_1^*	π_2^*
imidazole	−10.61	−10.17	−8.71	0.18	1.30
4,5-Me_2IM	−10.34	−9.90	−8.08	0.33	1.44

	$\pi_2+\pi_2$	$\pi_2-\pi_2$	n + n	n − n	$\pi_1+\pi_1$	$\pi_1-\pi_1$	$\pi_1^*+\pi_1^*$	$\pi_1^*-\pi_1^*$	$\pi_2^*+\pi_2^*$	$\pi_2^*-\pi_2^*$
BIM	−10.80	−10.67	−10.40	−10.23	−9.62	−8.10	−0.86	0.74	1.09	1.63
Me_4BIM	−10.50	−10.30	−10.07	−9.91	−8.83	−7.50	−0.64	0.99	1.31	1.83

	n,π^*	π,π^*	n,π^*	π,π^*
imidazole	4.37 (0.013)[a,b]	5.48 (0.184)	5.82 (0.003)	6.23 (0.091)
4,5-Me_2IM	4.34 (0.012)[b]	5.07 (0.203)	5.76 (0.003)	6.00 (0.110)

	n,π^*	π,π^*	π,π^*	π,π^*	π,π^*	π,π^*
BIM	4.05 (0.00)	4.12 (0.616)	4.18 (0.025)	5.37 (0.005)	5.84 (0.056)	5.91 (0.137)
Me_4BIM	4.12 (0.00)	3.81 (0.623)	4.25 (0.021)	4.99 (0.017)	5.62 (0.175)	5.67 (0.045)

[a] Calculated oscillator strengths are given in parentheses. [b] Not observed experimentally.[13]

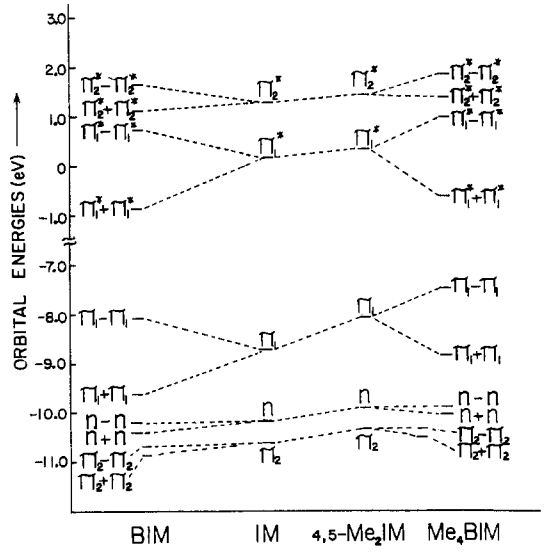

Figure 2. Correlation between the calculated frontier orbital energies of imidazole (IM), 4,5-dimethylimidazole (4,5-Me_2IM), 2,2′-biimidazole (BIM), and 4,4′,5,5′-tetramethyl-2,2′-biimidazole (Me_4BIM).

ligand $\pi \rightarrow \pi^*$ absorption and the n, π_1, π_2(imidazole) → Cu(II) LMCT absorptions of the Cu(II)–ligand complex are expected to red shift as a consequence of 4,5-dialkylation. Experimentally, these red shifts amount to ~3000 cm^{-1} for the $\pi \rightarrow \pi^*$ absorption and ~5000 cm^{-1} for the LMCT absorptions.[40]

The BIM and Me_4BIM ligands are comprised respectively of unsubstituted imidazole and 4,5-dimethylimidazole joined at ring position 2 by C–C bonds. A correlation of the calculated (INDO/S) frontier orbital energies for unsubstituted and 4,5-dimethylated imidazoles and biimidazoles is presented as Figure 2; the calculated orbital and excited-state energies are summarized in Table IV. The biimidazole MO's consist of plus and minus combinations of the orbitals supplied by the two imidazole fragments. Quantitatively, as might be predicted from the substantial 2p(π) coefficient of the π_1 orbital on the carbon atom that links the imidazole fragments, the $\pi_1 - \pi_1/\pi_1 + \pi_1$ splitting (1.52 eV for BIM and 1.33 eV for Me_4BIM) is considerably greater than the $\pi_2 - \pi_2/\pi_2 + \pi_2$ and n − n/n + n splittings (~0.2 eV) calculated for either ligand. Similarly, the imidazole π^*-orbital splitting results in considerably larger energy separation in the orbitals formed by the LUMO's ($\pi_1^* \approx 1.5$ eV) than in the orbitals formed from the higher lying π_2^* orbital (~0.5 eV); the former has its largest coefficient at the linking carbon atom, whereas the π_2^* orbital has only a modest coefficient at that position. Figure 2 indicates that, relative to imidazole, BIM is expected to exhibit ligand-localized $\pi \rightarrow \pi^*$ as well as $\pi \rightarrow$ Cu(II) LMCT absorptions at considerably lower energies. Owing to the electronic effects of methylation, the corresponding absorptions of Me_2IM and Me_4BIM are expected to be red shifted from those exhibited by their respective imidazole and BIM analogues.

Since neither BIM nor Me_4BIM are appreciably soluble in either H_2O or the common organic solvents, electronic spectral studies of the ligand transitions were performed with use of methanolic solutions of the soluble $Zn(BIM)_2 \cdot 2NO_3$ and $Zn(Me_4BIM)_2 \cdot 2NO_3$ complexes. Prior studies indicated that the $\pi \rightarrow \pi^*$ absorptions of imidazole and several 4,5-dialkylimidazoles were not perturbed significantly by complexation to Zn(II).[13] Methanolic $Zn(NO_3)_2 \cdot 6H_2O$ exhibits a very weak ($\epsilon \approx 10$) absorption at ~33 000 cm^{-1} along with a steep absorption edge at ~41 000 cm^{-1}. The lowest energy absorption of $Zn(BIM)_2 \cdot 2NO_3$ (Table V) occurs at 33 000 cm^{-1} (ϵ = 24 000) and is flanked by more intense and higher energy absorptions at 35 000 and 35 900 cm^{-1}. The INDO/S calculations (Table IV) predict a highly intense (f = 0.616) $\pi \rightarrow \pi^*$ absorption for planar BIM at 4.12 eV (33 200 cm^{-1}), which is very close in energy to a much weaker (f = 0.025) π,π^* transition. Accordingly, we assign these absorptions of $Zn(BIM)_2 \cdot 2NO_3$ as BIM $\pi \rightarrow \pi^*$ transitions. These transitions, as predicted, are considerably red shifted from the lowest energy $\pi \rightarrow \pi^*$ absorption ($\epsilon \approx 6900$) exhibited by free imidazole at 48 500 cm^{-1} (6.01 eV).

Corresponding absorptions, red shifted by ~3000 cm^{-1}, are exhibited by methanolic $Zn(Me_4BIM)_2 \cdot 2NO_3$ at 32 000 and 32 800 cm^{-1} and are assigned similarly as Me_4BIM $\pi \rightarrow \pi^*$ transitions. These spectra (Figure 6) also indicate the presence of shoulders removed to both higher and lower frequencies from the peaks above. The INDO/S calculations predict an intense (f = 0.623) ligand π,π^* excited state at 3.81 eV (30 700 cm^{-1}) and a less intense state at 4.25 eV (34 300 cm^{-1}, f = 0.021). The appearance of two closely spaced, intense peaks in the experimental spectra might result primarily from an inequivalence of the two Me_4BIM ligands, even in solution. Appearance of the shoulders is somewhat more difficult to understand. They may arise from interactions between the ligand π systems, or they may be related to the degree of planarity of the ligands. For example, a dihedral angle of 15° between the two rings in BIM leads to a calculated fourfold increase in the intensity of the weaker, high-energy band (f = 0.1) at the expense of the much stronger, lower lying transition (f = 0.5).

Electronic Structural Aspects of 1–6. Our main concern in this section is to identify the lowest energy biimidazole → Cu(II) LMCT absorptions and note their response to changes in energies of the upper occupied ligand orbitals. The higher

Table V. Summary of Electronic Spectral Results and Assignments

compd	soln (298 K)[a] ν, cm^{-1}	soln (298 K)[a] ϵ	mull(80 K) ν, cm^{-1}	assignt
$Zn(BIM)_2 \cdot 2NO_3$	35 800	48 000		ligand $\pi \rightarrow \pi^*$
	35 000	41 600		
	33 000 (sh)	~24 000		
$Cu(BIM)_2 \cdot 2NO_3$ (5)	35 500	56 500		ligand $\pi \rightarrow \pi^* + (\pi_1 + \pi_1) \rightarrow$ Cu(II)
	34 500	55 000	~30 000 (br)	
	32 500 (sh)	30 000		
	25 600	71	~23 300 (br)	$(\pi_1 - \pi_1) \rightarrow$ Cu(II)
	~13 800 (br)	38	~12 000 (br)	LF
$Zn_{0.9}Cu_{0.1}(BIM)_2 \cdot 2NO_3$ (6)			~31 000 (br)	ligand $\pi \rightarrow \pi^* + (\pi_1 + \pi_1) \rightarrow$ Cu(II)
			26 300	$(\pi_1 - \pi_1) \rightarrow$ Cu(II)
			~14 300 (br)	LF
$Zn(Me_4BIM)_2 \cdot 2NO_3$	32 800	68 000		ligand $\pi \rightarrow \pi^*$
	32 000 (sh)	~56 000		
	30 500 (sh)	~32 000		
$Cu(Me_4BIM)_2 \cdot 2NO_3$ (1)	32 600 (br)	70 000	~29 400	ligand $\pi \rightarrow \pi^* + (\pi_1 + \pi_1) \rightarrow$ Cu(II)
	26 000	52	~25 000 (sh)	$(\pi_1 + \pi_1) \rightarrow$ Cu(II)
	20 200	57	19 600	$(\pi_1 - \pi_1) \rightarrow$ Cu(II)
	~12 000 (br)	57	13 300	LF
			9 400	LF
$Zn_{0.9}Cu_{0.1}(Me_4BIM)_2 \cdot 2NO_3$ (2)			~28 600 (br)	ligand $\pi \rightarrow \pi^* + (\pi_1 + \pi_1) \rightarrow$ Cu(II)
			~25 000 (sh)	
			19 600	$(\pi_1 - \pi_1) \rightarrow$ Cu(II)
			13 300	LF
			~10 000	LF
$Zn(BIBENZ)_2 \cdot 2NO_3$	32 900	67 200		ligand $\pi \rightarrow \pi^*$
	~32 100 (sh)	~64 000		
	~30 200 (sh)	~32 800		
$Cu(BIBENZ)_2 \cdot 2NO_3$ (3)	31 500	76 800	~30 300 (br)	ligand $\pi \rightarrow \pi^*$
	29 400	46 000		
	~25 000 (sh)	~170	~25 000 (sh)	$(\pi_1 + \pi_1) \rightarrow$ Cu(II)
	20 800	100	20 400	$(\pi_1 - \pi_1) \rightarrow$ Cu(II)
	13 600	54	14 100	LF
$Zn_{0.9}Cu_{0.1}(BIBENZ)_2 \cdot 2NO_3$ (4)			~29 400 (br)	ligand $\pi \rightarrow \pi^*$
			~23 800 (sh)	$(\pi_1 + \pi_1) \rightarrow$ Cu(II) or $(\pi_1 - \pi_1) \rightarrow$ Cu(II)
			13 200	LF

[a] All solution spectra were measured in CH_3OH. The concentration of complexes 1–6 was 0.012 M. Due to the poor solubilities of the free ligands, their solution spectra were measured as the soluble $Zn(ligand)_2 \cdot 2NO_3$ complexes (0.005 M). All ϵ's are reported per mole of complex.

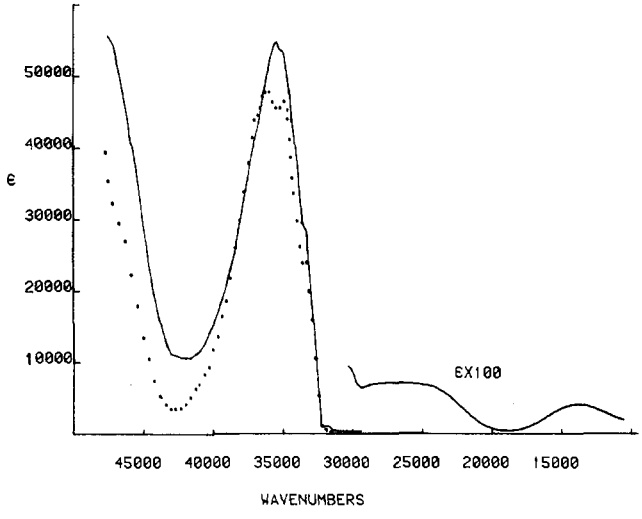

Figure 3. Electronic spectra of $Cu(BIM)_2 \cdot 2NO_3$ at 298 K as a 0.012 M solution in methanol (—). Reference near-UV spectra of the insoluble BIM ligand were obtained from a 0.005 M solution of the soluble $Zn(BIM)_2 \cdot 2NO_3$ complex (···).

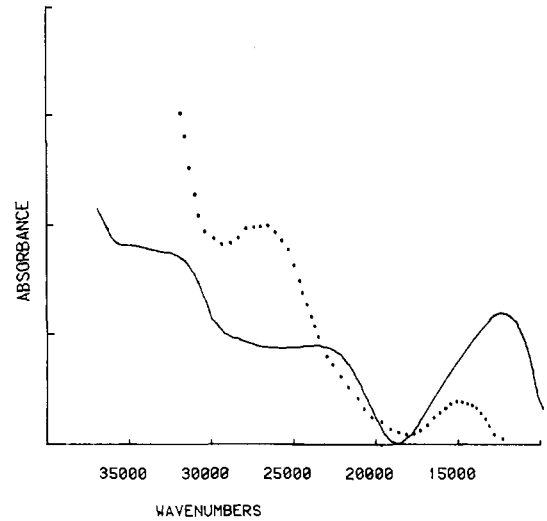

Figure 4. Electronic spectra at 80 K of $Cu(BIM)_2 \cdot 2NO_3$ (—) and $Zn_{0.9}Cu_{0.1}(BIM)_2 \cdot 2NO_3$ (···) as mineral oil mulls.

energy LMCT absorptions are obscured by the relatively intense ligand $\pi \rightarrow \pi^*$ absorptions, and the LF absorptions of pentacoordinate Cu(II) complexes already have been well characterized by other workers.[42,43]

The electronic spectra of the parent BIM ligand and its Zn(II) and Cu(II) complexes are summarized in Table V and

(42) Hathaway, B. J.; Procter, I. M.; Slade, R. C.; Tomlinson, A. A. G. *J. Chem. Soc. A* **1969**, 2219–24.

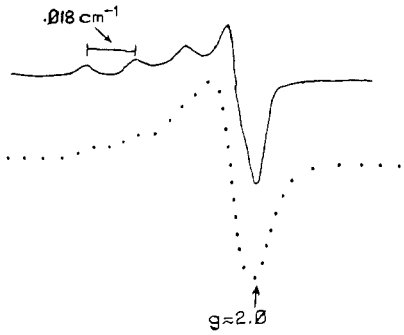

Figure 5. Low-temperature (80 K) X-band ESR spectra of $Cu(BIM)_2 \cdot 2NO_3$ (~0.005 M) in CH_3OH (—) and polycrystalline $Zn_{0.9}Cu_{0.1}(BIM)_2 \cdot 2NO_3$ (···).

Table VI. Summary of ESR Spectral Results[a]

compd[b]	$g_\perp$	$g_\parallel$ (or g)	$10^{-4}A_\parallel$, cm^{-1}
1 (CH_3OH)	2.091	2.273	116
2 (polycrystalline)	2.095	2.27	122
3 (CH_3OH)	2.095	2.260	98
4 (polycrystalline)	2.10	2.28	115
5 (polycrystalline)		2.06	
5 (CH_3OH)	2.003	2.24	182
6 (polycrystalline)	2.063	2.25	163

[a] All spectra were measured at 80 K. Frozen CH_3OH solutions were ~0.005 M in complex at room temperature. [b] See Table V for compound-numbering scheme.

presented as Figures 3 and 4. The solution spectra of $Zn(BIM)_2 \cdot 2NO_3$ reveal that the onset of the intense BIM $\pi \rightarrow \pi^*$ absorptions occurs at ~32 000 cm^{-1}. Two absorptions at lower energies are exhibited by methanolic $Cu(BIM)_2 \cdot 2NO_3$ (**5**). Bis Cu(II) complexes of related bidentate nitrogen donor ligands such as bpy exhibit one or more LF absorptions whose maxima span the 9200–15 600-cm^{-1} energy range depending upon the details of the CuN_4X (X = Cl, OH_2, ONO_2) coordination geometries. The broad, weak (ϵ = 38) absorption exhibited by methanolic **5** at ~13 800 cm^{-1} accordingly is assigned as the expected LF band. A second weak (ϵ = 71) absorption at 25 600 cm^{-1} is well removed toward higher energy from the characteristic region of LF absorptions and is assigned as the lowest energy BIM ($\pi_1 - \pi_1$) → Cu(II) LMCT absorption. Possible structural reasons for the weakness of this absorption are presented below in the analysis of the spectra exhibited by the crystallographically characterized complex **1**. The mull spectrum (Figure 4) of **5** reveals that the LF absorption has red shifted to ~12 000 cm^{-1} and indicates that the coordination geometries of methanolic and polycrystalline **5** differ in some respect. Presumably associated with the lowering of the Cu(II) d vacancy in polycrystalline **5** is a comparable red shift (~2300 cm^{-1}) in the ($\pi_1 - \pi_1$) → Cu(II) LMCT absorption. An additional feature in the mull spectra at ~30 000 cm^{-1} is appropriate in energy for the expected BIM ($\pi_1 + \pi_1$) → Cu(II) LMCT absorption (see below) but cannot be assigned with confidence due to neighboring and probably overlapping ligand $\pi \rightarrow \pi^*$ absorptions. The polycrystalline Cu(II)-doped complex **6** exhibits LF and LMCT absorptions at energies close to those observed for methanolic **5**. The implied structural similarity of these Cu(II) chromophores also is supported by ESR data. Both methanolic **5** and polycrystalline **6** exhibit similar tetragonal ESR spectra (Figure 5) from which similar $g_\perp$, $g_\parallel$, and $A_\parallel$ values may be extracted (Table VI). Neat polycrystalline **5** is too concentrated magnetically for structurally useful ESR studies to be performed.

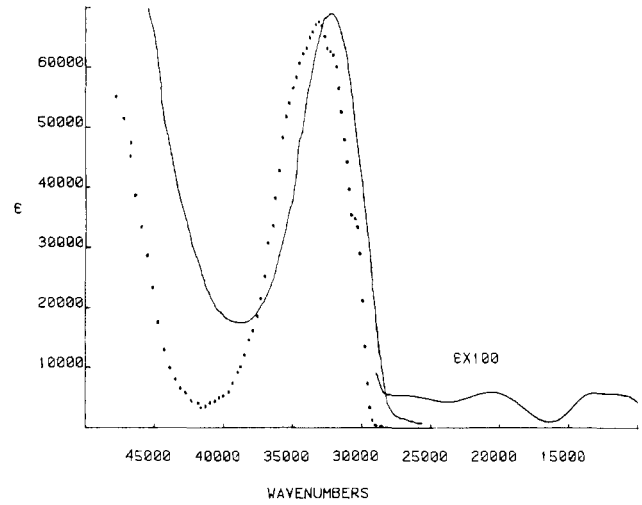

Figure 6. Electronic spectra of **1** at 298 K as a 0.012 M solution in methanol (—). Reference near-UV spectra of the insoluble Me_4BIM ligand were obtained from a 0.005 M solution of the soluble $Zn(Me_4BIM)_2 \cdot 2NO_3$ complex (···).

The complexes of Me_4BIM are considered next. As noted above, the approximately 3000-cm^{-1} red shift of the ligand $\pi \rightarrow \pi^*$ absorptions (Table V) relative to those of the parent BIM ligand is an expected consequence of ring methylation. Methanolic $Cu(Me_4BIM)_2 \cdot 2NO_3$ (**1**) exhibits three absorptions at lower energies than the Me_4BIM absorption edge at ~30 000 cm^{-1}. A broad unresolved absorption at ~12 000 cm^{-1} (ϵ = 57) is assigned to LF absorption by analogy to those assigned by other workers for $[Cu(bpy)_2X]^+$ (X = Cl, NO_3) chromophores.[42,43] The additional absorptions well removed toward higher energy at 20 200 cm^{-1} (ϵ = 57) and 26 000 cm^{-1} (ϵ = 52) are assigned respectively to Me_4BIM ($\pi_1 - \pi_1$) → Cu(II) and ($\pi_1 + \pi_1$) → Cu(II) LMCT. These absorptions are weaker by a factor of ~30 and red shifted by ~8000 cm^{-1} relative to the π(ligand) → Cu(II) LMCT absorptions reported for tetrakis Cu(II) complexes of simple imidazoles.[13,40] For example, the lowest energy LMCT ($\pi_1 \rightarrow$ Cu(II)) of various Cu(4,5-dialkylimidazole)$_4^{2+}$ complexes occurs at ~28 600 cm^{-1} ($\epsilon \approx$ 1500). However, the HOMO of Me_4BIM is calculated to be 0.58 eV less stable than the HOMO (π_1) of 4,5-dimethylimidazole (Table IV). For this reason alone, the ($\pi_1 - \pi_1$) → Cu(II) LMCT absorption of **1** should be red shifted by ~4700 cm^{-1} from the $\pi_1 \rightarrow$ Cu(II) LMCT absorptions exhibited by Cu(4,5-dialkylimidazole)$_4^{2+}$ chromophores. An additional red shift (of unknown magnitude) may be expected due to the lower energy of the Cu(II) d vacancy ($d_{x^2-y^2}$) in **1** (LF absorptions at ~12 000 cm^{-1}) relative to those of the Cu(4,5-dialkylimidazole)$_4^{2+}$ chromophores (LF absorptions at ~16 500 cm^{-1}). The calculated separation between the ($\pi_1 - \pi_1$) and ($\pi_1 + \pi_1$) orbitals in uncomplexed Me_4BIM is 1.33 eV (10 700 cm^{-1}). With use of a simple one-electron picture (i.e. the contributions of coulombic integrals, electron correlation effects, etc. being ignored) the "calculated" difference in ($\pi_1 - \pi_1$) → Cu(II) and ($\pi_1 + \pi_1$) → Cu(II) LMCT energies is ~10 700 cm^{-1}, compared with the observed differences of ~6000 cm^{-1} based upon our assignment scheme.

The weakness of these $Me_4BIM \rightarrow$ Cu(II) LMCT absorptions may originate in the structural features observed for crystalline **1**. Qualitatively, the LMCT absorptions exhibited by crystalline **1** and the Cu(II)-doped zinc complex **2** (Figure 7) *approximately* are as intense as the LF absorptions (i.e., they do not differ by an order of magnitude). A quantitative estimate of the relative band intensities may be obtained from the extinction coefficients presented in Table V. We have

(43) Harrison, W. D.; Kennedy, D. M.; Power, M.; Sheahan, R.; Hathaway, B. J. *J. Chem. Soc., Dalton Trans.* **1981**, 1556–64.

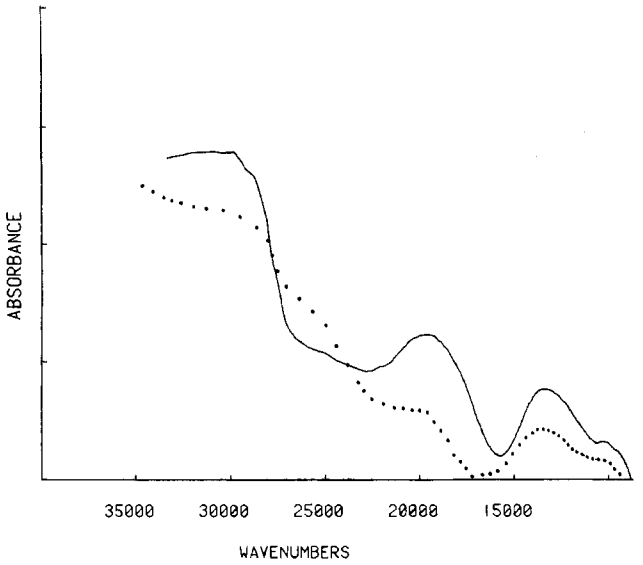

Figure 7. Electronic spectra at 80 K of **1** (—) and **2** (···) as mineral oil mulls.

suggested that the relatively large intensities of the π_1,π_2(imidazole) → Cu(II) LMCT absorptions ($\epsilon \approx 1500$) exhibited by Cu(4,5-dialkylimidazole)$_4^{2+}$ chromophores are associated with steric effects arising from the alkyl groups. These bulky ring substituents serve to orient the imidazole rings approximately perpendicular to the CuN_4 units. This expectation has been verified by a crystallographic study of the Cu(1,4,5-trimethylimidazole)$_4$·2ClO_4 complex; dihedral angles between the imidazole rings and the planar CuN_4 unit were observed to be 75.5 and 75.7°.[40] Group theoretical selection rules indicate that for tetragonal complexes ($d_{x^2-y^2}$ ground state) the π(imidazole) → Cu(II) LMCT absorptions should be polarized in the CuN_4 plane (x,y), when the imidazole rings are oriented perpendicular to the CuN_4 unit, and polarized normal to the CuN_4 plane (z), when the imidazole rings are coplanar with the CuN_4 unit. In addition, only the former orientation should make intensity stealing from the strongly allowed in-plane (x,y) polarized n(imidazole) → Cu(II) LMCT absorptions possible. A reduction in chromophore symmetry to square pyramidal would not be expected to alter these expectations significantly. Of the two Me_4BIM ligands in **1**, the one containing N(1) and N(4) (Figure 1) exhibits a dihedral angle of 97.7° relative to the CuN(4)N(5)N(8)O(1) equatorially bonded unit whereas the ligand containing N(5) and N(8) exhibits a corresponding angle of only 2.9°. Moreover, the imidazole ring containing N(1) is bound apically and has reduced overlap with the Cu(II) d vacancy. Thus, only one of the four imidazole rings in **1** is properly oriented for ligand ($\pi_1 - \pi_1$) → Cu(II) LMCT absorption. Since the simple Cu(4,5-dialkylimidazole)$_4^{2+}$ chromophores exhibit π(imidazole) → Cu(II) LMCT absorptions having an intensity of ~400 *per ligand*, the presence of only one strategically oriented imidazole ring in **1** might reasonably contribute to the weakness ($\epsilon \approx 50$) of the observed LMCT absorptions.

The electronic spectra of methanolic **1** (Figure 6) and of the polycrystalline complexes **1** and **2** (Figure 7) are very similar. Moreover, the ESR spectra (Figure 8) and parameters (Table VI) of methanolic **1** and the polycrystalline Cu(II)-doped complex **2** nearly are identical. These spectroscopic data indicate that the Cu(II) chromophore crystallographically characterized in neat **1** essentially is retained in both methanol and solid-state solutions. Apparently, the doped Cu(II) chromophore retains the structural features of neat **1** as opposed to adopting the somewhat different coordination geometry observed for the dominant Zn(Me_4BIM)$_2$·2NO_3 chromophore in **2**. This uncommon situation also has been noted

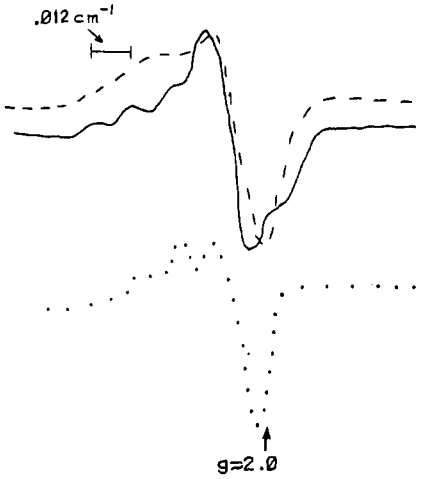

Figure 8. Low-temperature (80 K) X-band ESR spectra of **1** (polycrystalline (---) and ~0.005 M in CH_3OH (—)) and **2** (···).

for the M(dien)(bipyridylamine)·2NO_3 system (M = Cu, Zn).[44] The apparent near-isomorphism of **1** and **2** suggested by their identical space group and somewhat similar lattice parameters neither requires nor results in isostructural coordination geometries. The Cu(II) complex readily dopes into the lattice formed by the Zn(II) analogue yet clearly retains its own coordination geometry and associated electronic structural features.

Finally, the spectroscopic results for the various BIBENZ complexes (Tables V and VI) closely parallel those of the Me_4BIM complexes. Both ligands, as might be expected, exhibit nearly identical $\pi \rightarrow \pi^*$ absorptions. Both **1** and Cu(BIBENZ)$_2$·2NO_3 (**3**) exhibit similar LF and LMCT absorptions in methanolic solution and in mineral oil mull dispersions. Moreover, a Cu(II)-doped Zn(II) analogue may be prepared readily. Both methanolic **3** and Cu(II)-doped **4** exhibit similar ESR spectra and parameters (Table VI). In contrast to the Me_4BIM analogues, however, the ($\pi_1 - \pi_1$) → Cu(II) and ($\pi_1 + \pi_1$) → Cu(II) LMCT absorptions of **4** are not well resolved but presumably give rise to the spectral feature (shoulder) at ~23 800 cm^{-1}. This result may be due to a peculiar orientation of the BIBENZ rings in **4**. Further pursuit of this question would necessitate additional crystallographic studies, which are not planned at this time.

Conclusions

If the metal–O semibond arising from anisobidentate NO_3^- ligation is ignored, the CuN_4O unit of **1** and the ZnN_4O unit of **2** exhibit somewhat different distorted square-pyramidal coordination geometries; a major difference is the length of the M–N apical bonds. INDO/S calculations have revealed the energy relationships between the frontier BIM and Me_4BIM orbitals and those supplied by the individual imidazole and 4,5-dimethylimidazole subunits. The $\pi_1 - \pi_1$ and $\pi_1 + \pi_1$ BIM and Me_4BIM orbitals (where π_1 is the HOMO supplied by the imidazole subunit) are of particular spectroscopic interest. The red shifts of the BIM and Me_4BIM $\pi \rightarrow \pi^*$ absorptions and the energies and separations of the ($\pi_1 - \pi_1$) → Cu(II) and ($\pi_1 + \pi_1$) → Cu(II) LMCT absorptions are in harmony with the INDO/S results. Crystallographic studies, which indicate that only one imidazole ring in the [Cu(Me_4BIM)$_2$$ONO_2$]$^+$ chromophore may have a spectroscopically favorable orientation, provide a possible explanation for the weakness of the above LMCT absorptions. The Cu(II) chromophore in crystalline **1** is unusual in that it persists relatively unchanged in methanol solution and in the lattice of the Zn(II) analogue, which has a somewhat different co-

(44) Ray, N.; Hathaway, B. *J. Chem. Soc., Dalton, Trans* **1980**, 1105–11.

ordination geometry. **1**, Cu(II)-doped **2**, and methanolic **1** exhibit nearly identical electronic spectra, and the last two systems exhibit nearly identical ESR spectra. Similar behavior is exhibited by the corresponding complexes of BIBENZ.

Acknowledgment. This work was supported by the National Institutes of Health (Grant AM-16412 to H.J.S). We thank the Center for Computer and Information Services, Rutgers University, for providing computer time, and the Rutgers Research Council for partial support (to K.K.-J.).

Registry No. **1**, 87494-83-5; **2**, 87494-85-7; **3**, 87508-96-1; **4**, 87517-34-8; **5**, 87494-87-9; **6**, 87517-36-0; 4,5-Me_2Im, 2302-39-8; BIM, 492-98-8; Me_4BIM, 69286-06-2; BIBENZ, 87508-94-9; NH_3, 7664-41-7; imidazole, 288-32-4; 1,2-cyclohexanedione, 765-87-7; glyoxal, 107-22-2.

Supplementary Material Available: Tables of calculated hydrogen atom positions, anisotropic thermal parameters, observed and calculated structure factors, and deviations from least-squares planes for **1** and **2** (32 pages). Ordering information is given on any current masthead page.

Contribution from Chevron Research Company, Richmond, California 94802

High-Field ^{11}B NMR of Alkali Borates. Aqueous Polyborate Equilibria

CHRISTOPHER G. SALENTINE

Received March 3, 1983

The 127- and 160-MHz ^{11}B NMR spectra of aqueous solutions of $KB_5O_8{\cdot}4H_2O$, $K_2B_5O_8(OH){\cdot}2H_2O$, $K_2B_4O_7{\cdot}4H_2O$, and $NaB_5O_8{\cdot}5H_2O$ are reported. Separation of all three signals in solutions of the MB_5O_8 (M = Na, K) pentaborates resulted in calculation of the formation constants for $B(OH)_4^-$ and the polyborates $B_3O_3(OH)_4^-$ and $B_5O_6(OH)_4^-$. All solid samples yielded substantial concentrations of $B_3O_3(OH)_4^-$ and low-to-moderate concentrations of $B_5O_6(OH)_4^-$ in aqueous solution, both detected easily by their resonances at 13 and 1 ppm, respectively. The presence of $B_5O_6(OH)_4^-$ in solutions of pH up to 9.7 was unexpected. The $B_4O_5(OH)_4^{2-}$ ion, though certainly present at pH 9.7, was not detected in these studies. Variable-temperature spectra from 5 to 80 °C and concentration-dependent spectra supported previous observations of the dissociation of the polyborate complexes at high temperature or high dilution. The $B_5O_6(OH)_4^-$ ion gives one signal in its spectrum apparently due only to the tetrahedral boron atom. The trigonal boron resonances for this ion were not observed.

The structural and solution chemistry of the hydrated alkali and alkaline-earth borates remains a topic of current interest,[1] largely due to a history of conflicting reports that are not yet totally resolved. A variety of experimental methods have unequivocally established the existence of polyborate anions in aqueous solution;[2] these ions also occur as discrete entities in the solid state, but the relationship between solid and solution structures is complex due to rapid interconversions of polyborates in solution. The pioneering work of Ingri[3] yielded formation constants from potentiometric titration for the major species postulated to be present in solution. Spectroscopic techniques subsequently lent support with more direct evidence; aqueous polyborate equilibria were studied by ^{11}B NMR[4,5] and more recently by Raman spectroscopy.[6,7] The latter proved successful, and formation constants for $B_3O_3(OH)_4^-$, $B_4O_5(OH)_4^{2-}$, and $B_5O_6(OH)_4^-$ were reported:[6]

$$B(OH)_3 + OH^- \rightleftharpoons B(OH)_4^- \quad K_1 \qquad (1)$$

$$2B(OH)_3 + B(OH)_4^- \rightleftharpoons B_3O_3(OH)_4^- + 3H_2O \quad K_3 \qquad (2)$$

$$2B(OH)_3 + 2B(OH)_4^- \rightleftharpoons B_4O_5(OH)_4^{2-} + 5H_2O \quad K_4 \qquad (3)$$

$$4B(OH)_3 + B(OH)_4^- \rightleftharpoons B_5O_6(OH)_4^- + 6H_2O \quad K_5 \qquad (4)$$

Previous ^{11}B NMR studies[4,5] of the polyborate equilibria at 14 and 80 MHz were limited by the signal broadening typically associated with this method. We now report new ^{11}B NMR data at 127 and 160 MHz. The higher field strengths provided excellent resolution of signals with concomitant identification and quantification of species not previously possible by NMR. We also include the first variable-temperature ^{11}B NMR study of the polyborate equilibria. This report should clarify, at least in part, some of the conflicting data reported on aqueous polyborate chemistry over the past several decades.[1f]

Table I. ^{11}B NMR Data

compd	concn, M	temp, °C	chem shift, ppm[a] (% rel area)
$KB_5O_8{\cdot}4H_2O$	0.15	5	18.1 (63.1), 12.6 (29.7), 0.8 (7.2)
	0.15	25	17.9 (60.4), 12.8 (34.8), 0.9 (4.8)
	0.10	25	17.6 (66.6), 13.0 (31.6), 0.9 (1.8)
	0.05	25	16.7, 12.7
	satd	41	17.7, 13.0, 0.9
	satd	83	16.9, 1.7
$K_2B_5O_8(OH){\cdot}2H_2O$	0.2	22	11.7 (97.0), 0.9 (3.0)
	0.4	25	11.7 (91.0), 0.9 (9.0)
	satd	6	11.5, 0.6
	satd	61	12.7, 1.9
$K_2B_4O_7{\cdot}4H_2O$	0.2	5	11.9, 7.5 (98.4), 1.0 (1.6)
	0.2	25	12.2, 8.3 (99.0), 0.9 (1.0)
	0.4	25	11.6, 7.6 (98.2), 0.9 (1.8)
	0.6	41	10.0, 1.4
	0.6	61	10.3
	0.6	80	10.8
$NaB_5O_8{\cdot}5H_2O$	0.15	5	18.7 (65.6), 13.1 (26.1), 1.2 (8.3)
	0.15	25	18.2 (62.8), 13.0 (32.3), 1.1 (4.9)
	0.30	25	18.7 (62.8), 13.2 (24.6), 1.1 (12.6)
	0.40	25	18.9 (58.7), 13.2 (24.9), 1.0 (16.4)

[a] Referenced to external $Et_2O{\cdot}BF_3$; solvent is H_2O.

(1) (a) Christ, C. L.; Clark, J. R. *Phys. Chem. Miner.* **1977**, *2*, 59. (b) Wan, S. G. C.; Clark, J. R. *Am. Mineral.* **1978**, *63*, 160. (c) Corti, H.; et al. *J. Chem. Soc., Faraday Trans. 1* **1980**, *76*, 2179. (d) Silins, E.; Schwarz, E.; Ozolins, G. *J. Struct. Chem. (Engl. Transl.)* **1981**, *22*, 414. (e) Farmer, J. *Chem. Ind. (London)* **1982** (March 6), 145. (f) Farmer, J. B. *Adv. Inorg. Chem. Radiochem.* **1982**, *25*, 187–237.
(2) Mellor, J. W. "A Comprehensive Treatise on Inorganic and Theoretical Chemistry,"; Longmans, Green and Co.: London, 1980; Vol. 5, Part A, Supplement 1, pp 259–71, 409–17.
(3) Ingri, N. *Sven. Kem. Tidskr.* **1963**, *75*, 199 and references therein.
(4) Momii, R. K.; Nachtrieb, N. H. *Inorg. Chem.* **1967**, *6*, 1189.
(5) Smith, H. D., Jr.; Wiersema, R. J. *Inorg. Chem.* **1972**, *11*, 1152.
(6) Maya, L. *Inorg. Chem.* **1976**, *15*, 2179.
(7) Maeda, M.; et al. *J. Inorg. Nucl. Chem.* **1979**, *41*, 1217.

0020-1669/83/1322-3920$01.50/0